



Published in final edited form as:

*Ann Appl Stat.* 2015 December ; 9(4): 2153–2178. doi:10.1214/15-AOAS879.

## **BFLCRM: A BAYESIAN FUNCTIONAL LINEAR COX REGRESSION MODEL FOR PREDICTING TIME TO CONVERSION TO ALZHEIMER'S DISEASE\***

**Eunjee Lee<sup>†</sup>, Hongtu Zhu<sup>†</sup>, Dehan Kong<sup>†</sup>, Yalin Wang<sup>‡</sup>, Kelly Sullivan Giovanello<sup>†</sup>, and Joseph G Ibrahim<sup>†</sup> for the Alzheimer's Disease Neuroimaging Initiative**

<sup>†</sup>Departments of Statistics and Operation Research, Biostatistics, and Psychology and Biomedical Research Imaging Center, University of North Carolina at Chapel Hill, Chapel Hill, NC 27599, USA

<sup>‡</sup>School of Computing, Informatics, and Decision Systems Engineering Arizona State University Tempe, AZ 85287-8809 ylwang@asu.edu

### **Abstract**

The aim of this paper is to develop a Bayesian functional linear Cox regression model (BFLCRM) with both functional and scalar covariates. This new development is motivated by establishing the likelihood of conversion to Alzheimer's disease (AD) in 346 patients with mild cognitive impairment (MCI) enrolled in the Alzheimer's Disease Neuroimaging Initiative 1 (ADNI-1) and the early markers of conversion. These 346 MCI patients were followed over 48 months, with 161 MCI participants progressing to AD at 48 months. The functional linear Cox regression model was used to establish that functional covariates including hippocampus surface morphology and scalar covariates including brain MRI volumes, cognitive performance (ADAS-Cog), and APOE status can accurately predict time to onset of AD. Posterior computation proceeds via an efficient Markov chain Monte Carlo algorithm. A simulation study is performed to evaluate the finite sample performance of BFLCRM.

---

\*The research of Drs. Zhu and Ibrahim was supported by NIH grants RR025747-01, GM70335, CA74015, P01CA142538-01, MH086633, EB005149-01 and AG033387. The content is solely the responsibility of the authors and does not necessarily represent the official views of the NIH. Data used in preparation of this article were obtained from the Alzheimer's Disease Neuroimaging Initiative (ADNI) database (adni.loni.usc.edu). As such, the investigators within the ADNI contributed to the design and implementation of ADNI and/or provided data but did not participate in analysis or writing of this report. A complete listing of ADNI investigators can be found at: [http://adni.loni.usc.edu/wpcontent/uploads/how\\_to\\_apply/ADNI\\_Acknowledgement\\_List.pdf](http://adni.loni.usc.edu/wpcontent/uploads/how_to_apply/ADNI_Acknowledgement_List.pdf).

Address for correspondence and reprints: Hongtu Zhu, Ph.D., hzhu@bios.unc.edu, eunjee2@live.unc.edu, kongd@live.unc.edu, kgio@email.unc.edu, ibrahim@bios.unc.edu

#### **SUPPLEMENTARY MATERIAL**

Supplement A: Supplement to "BFLCRM: A Bayesian Functional Linear Cox Regression Model for Predicting Time to Conversion to Alzheimer's Disease" (doi: COMPLETED BY THE TYPESETTER; SuppBFLCRM.pdf). This supplementary document contains additional results of ADNI-1 data analysis. Sensitivity analysis results for the full model were discussed for the purpose of evaluating the robustness of prior choice. As additional information, we interpreted the posterior quantities associated with the reduced models, Model 1, 2, and 3.

*MSC 2010 subject classifications:* Primary 60K35, 60K35; secondary 60K35

## Keywords

Alzheimer's disease; functional principal component analysis; hippocampus surface morphology; mild cognitive impairment; proportional hazard model

---

## 1. Introduction

Alzheimer's Disease (AD) is a firmly incurable and progressive disease [14]. In the pathology of AD, mild cognitive impairment (MCI) is a clinical syndrome characterized by insidious onset and gradual progression, and commonly arising as a result of underlying neurodegenerative pathology [26]. Since MCI is considered as a risk state for AD, a major research focus in recent years has been to delineate a set of biomarkers that provide evidence of such a neurodegenerative pathology in living individuals, with the goal of specifying the likelihood that the pathophysiological process is due to Alzheimer's disease (MCI due to AD; MCI-AD) and will lead to dementia within a few years [1]. Accordingly, increasing attention has been devoted to investigate the utility of various imaging, genetic, clinical, behavioral, and fluid data to predict the conversion from MCI to AD.

Several studies have utilized a small subset of biosignatures and then assessed the relative importance of different modalities in predicting the diagnostic change from MCI to AD [12, 21, 58, 61, 80]. For example, in [12], the authors simultaneously examined multiple features from different modalities, including structural magnetic resonance imaging (MRI) morphometry, cerebrospinal fluid biomarkers, and neuropsychological measures to assess an optimal set of predictors of conversion from MCI to AD. They observed that structural changes within the medial temporal lobe (MTL), particularly the hippocampus, as well as performance on cognitive tests that rely on MTL integrity (i.e., episodic memory), were good predictors of MCI to AD conversion.

Recently, most researchers have turned to the analysis of longitudinal data to assess the dynamic changes of various biomarkers associated with the MCI-to-AD transition across time. To begin, a prominent neural correlate of MCI-AD is volume loss within the MTL, especially within the hippocampus and entorhinal cortex [19], with increasing atrophy in these structures from normal aging to MCI to AD [54]. Longitudinal studies of individuals with MCI-AD have also highlighted the importance of assessing MTL changes in tracking the progression of MCI to AD. For example, several studies have documented diminished baseline hippocampal and entorhinal volumes that are associated with an increased likelihood of progressing to clinical dementia [29, 41]. Additionally, several modalities of disease indicators have been studied to assess progression to AD, including neuroimaging markers [61, 75, 79], biomedical markers [65], and neuropsychological assessments [55]. Finally, a number of structural MRI studies, covering region of interest (ROI), volume of interest, voxel-based morphometry, and shape analysis have reported that the degree of atrophy in several brain regions, such as the hippocampus and entorhinal cortex, is not only sensitive to disease progression, but also predicts MCI conversion [10, 16, 48].

Despite the importance of these investigations, a central question remains. Namely, how do we accurately predict the time to conversion in individuals who harbor AD pathology, as

well as determine the optimal early markers of conversion? In [73], 148 MCI subjects were used to identify the most predictive neuropsychological measures. In [44], 139 MCI subjects in ADNI-1 were used to evaluate the predictive power of brain volume, ventricular volume, hippocampus volume, APOE status, cerebrospinal fluid (CSF) biomarkers, and behavioral scores. Their results show a moderately accurate prediction with the value of an area under the curve of 0.757 at 36 months, whereas they found that baseline volumetric MRI and behavioral scores were selectively predictive. Finally, in [13], 381 MCI subjects from ADNI 1 were examined to evaluate several biomarkers for predicting MCI to AD conversion including spatial patterns of brain atrophy, ADAS-Cog, APOE genotype, and cerebrospinal fluid (CSF) biomarkers. Their findings suggest that a combination of spatial patterns of brain atrophy and ADAS-Cog offers good predictive power of conversion from MCI to AD, whereas APOE genotype did not significantly improve prediction. To the best of our knowledge, no prior study has examined the role of functional covariates including hippocampus surface morphology in predicting time to conversion from MCI to AD with/without adjusting for low-dimensional behavioral and clinical measures.

To assess the predictability of hippocampus surface morphology in survival models, we develop a Bayesian functional linear Cox regression model (BFLCRM) with both functional and scalar covariates. The BFLCRM integrates a Cox proportional hazard regression and functional linear model into a single framework. First, BFLCRM can be an important extension of various statistical models including parametric, semiparametric and nonparametric models for handling survival response data and scalar covariates. See overviews of various survival models in [24, 33, 40] and the references therein. Recent advances in computation and prior elicitation have made Bayesian analyses of these survival models with scalar covariates feasible. For instance, nonparametric prior processes including the gamma process prior, the Beta process model, the correlated gamma process, and the Dirichlet process prior have been developed as the prior distribution of the baseline cumulative hazard function [33, 70]. Second, BFLCRM can be an important extension of various functional linear models for handling discrete or continuous response data and functional covariates. The existing literature focuses on the development of frequentist methods for functional linear models. Some examples include [23, 38, 59, 60, 78] and the references therein. Third, BFLCRM can be regarded as an important extension of high-dimensional survival models. However, most high-dimensional survival models focus on the identification of a small set of covariates and their overall effect on time-to-event outcomes [5, 39, 43]. These approaches can be sub-optimal for high-dimensional imaging data, since the effect of imaging data on clinical data and other imaging data is often *non-sparse*, which makes it notoriously difficult for many existing regularization methods [20, 74].

In Section 2, we will introduce BFLCRM and its associated Bayesian estimation procedure. In Section 3, we will introduce the NIH Alzheimer's Disease Neuroimaging Initiative (ADNI) dataset and illustrate the use of BFLCRM in the prediction of time to conversion from MCI to AD by using both functional and scalar covariates. In Section 4, we conduct simulation studies to examine the finite sample performance of BFLCRM. In Section 5, we interpret the findings obtained from the analysis of ADNI dataset.

## 2. Bayesian Functional Linear Cox Regression Models

### 2.1. Setup.

Consider imaging, genetic, and clinical data from  $n = 346$  independent MCI patients in ADNI-1. For the  $i$ -th MCI patient, we observe a possibly right censored time to conversion to AD, denoted by  $y_i$ . Specifically,  $y_i = T_i \wedge C_i$  is the minimum of the censoring time  $C_i$  and the transition time  $T_i$  and  $v_i = \mathbf{1}(y_i = T_i)$ , where  $\mathbf{1}(\cdot)$  is an indicator function. Moreover, we observe a  $p \times 1$  vector of scalar covariates, denoted by  $\mathbf{x}_i = (x_{i1}, \dots, x_{ip})^T$ , and a functional covariate, denoted by  $Z_i(\cdot)$ , on a compact set  $\mathcal{S}$ . In this paper, we focus on the noninformative censoring setting such that  $T_i$  and  $C_i$  are conditionally independent given all covariates of interest. The scalar covariates of interest include age at baseline, length of education, gender, handedness, marital status, retirement, and the well-known Apolipoprotein E (APOE) SNPs. The APOE has three major forms,  $\epsilon 2$ ,  $\epsilon 3$ , and  $\epsilon 4$ , where  $\epsilon 3$  is the most common form. The functional covariate of interest is the hippocampus surface morphology. Figure 1 shows the example hippocampus surface morphology data in ADNI-1 data.

Our problems of interest are to establish the likelihood of conversion to Alzheimer's disease (AD) in 346 MCI patients enrolled in the ADNI-1 and to select the optimal early markers of conversion from both the scalar covariates and the functional covariate. With the sole presence of  $\mathbf{x}_i$ , it is common to consider Cox's proportional hazards model [11], which assumes that the conditional hazard function of  $y_i$  given  $\mathbf{x}_i$  is given by

$$h(y|\mathbf{x}_i) = h_0(y) \exp(\mathbf{x}_i^T \boldsymbol{\beta}) = h_0(y) \exp\left(\sum_{k=1}^p x_{ik} \beta_k\right), \quad (2.1)$$

where  $\boldsymbol{\beta} = (\beta_1, \dots, \beta_p)^T$  is a  $p \times 1$  vector of regression coefficients and  $h_0(\cdot)$  is an unknown baseline hazard function. However, the Cox proportional hazards model (2.1) does not incorporate the effect of the functional covariate  $Z_i(\cdot)$  on the time to conversion.

### 2.2. Model Formulation

We propose a Bayesian functional linear Cox regression model with three main ingredients for handling both functional and scalar covariates as a natural extension of (2.1). Based on this formulation, we take a Bayesian approach to estimate the parameters of interest.

In the first component of BFLCRM, it is assumed that the hazard function of  $y_i$  given  $(\mathbf{x}_i, Z_i(\cdot))$  is given by

$$h(y|\mathbf{x}_i, Z_i(\cdot)) = h_0(y) \exp\left(\sum_{k=1}^p x_{ik} \beta_k + \int_{\mathcal{S}} \gamma(s) (Z_i(s) - \mu(s)) ds\right), \quad (2.2)$$

where  $\mu(s)$  is the mean function of  $Z_i(s)$  and  $\gamma(\cdot)$  is an unknown coefficient function, a square integrable function on  $\mathcal{S}$ .

The second component of BFLCRM is the functional principal component analysis (fPCA) model of the  $Z_i(\cdot)$ 's. It is assumed that the  $Z_i(s)$ 's are square integrable random functions and  $W_i(s)$  are measured at a set of grid points in  $\mathcal{S}$  with measurement errors such that

$$W_i(s) = Z_i(s) + \epsilon_i(s) = \mu(s) + \bar{Z}_i(s) + \epsilon_i(s), \quad (2.3)$$

where  $\bar{Z}_i(s)$  characterizes individual functional variations from  $\mu(s)$ . The  $\epsilon_i(s)$ 's are measurement errors with mean zero and variance  $\sigma_\epsilon^2(s)$  at each  $s$  and independent of each other for  $s \neq s'$ . Moreover,  $\mu(s)$  can be consistently estimated by  $\hat{\mu}(s) = \sum_{i=1}^n W_i(s) / n$ .

It is assumed that  $Z_i(s)$  and  $\epsilon_i(s)$  are independent of each other and the covariance function of  $\{\bar{Z}_i(s) : s \in \mathcal{S}\}$ , denoted by  $K(s, s') = E\{\bar{Z}(s) \bar{Z}(s')\}$ , is continuous on  $\mathcal{S} \times \mathcal{S}$ . According to Mercer's theorem,  $K(s, s')$  also admits a spectral decomposition

$$K(s, s') = \sum_{j=1}^{\infty} \psi_j \phi_j(s) \phi_j(s'), \text{ where } (\psi_j, \phi_j(s))\text{'s are the eigenvalue-eigenfunction pairs of } K(s, s') \text{ such that } \{\psi_j : j \geq 1\} \text{ are the eigenvalues in decreasing order with } \sum_{j=1}^{\infty} \psi_j^2 < \infty.$$

Thus,  $\bar{Z}_i(s)$  admits the Karhunen-Loeve expansion as  $\bar{Z}_i(s) = \sum_{j=1}^{\infty} \xi_{ij} \phi_j(s)$ , where  $\xi_{ij}$  are referred to functional principal component (fPC) scores and  $\xi_{ij} = \int_{\mathcal{S}} \bar{Z}_i(s) \phi_j(s) ds$  are uncorrelated random variables with mean zero and variance  $\psi_j = E(\xi_{ij}^2)$ . To estimate  $\xi_{ij}$  based on the observed covariate functions  $W_i(s)$ , we first employ the cubic smoothing spline [30] to estimate the underlying signal  $Z_i(s)$ . We then use the sample mean and covariance functions of the estimated  $Z_i(s)$  to estimate  $\mu(s)$  and  $K(s, s')$ . Subsequently, we estimate  $\phi_j(s)$  and  $\xi_{ij}$  for all  $i, j \leq n$ .

The third component of the FLCRM is an approximation of  $\int_{\mathcal{S}} \gamma(s) \bar{Z}(s) ds$ . Since the eigenfunctions  $\phi_j(\cdot)$  form a complete orthonormal system on the space of square-integrable functions on  $\mathcal{S}$ , the covariate function  $\gamma(s)$  can be expanded as

$$\gamma(s) = \sum_{j=1}^{\infty} \phi_j(s) \gamma_j \quad \text{with} \quad \sum_{j=1}^{\infty} \gamma_j^2 < \infty. \quad (2.4)$$

Therefore, we have

$$\int_{\mathcal{S}} \bar{Z}_i(s) \gamma(s) ds = \sum_{j=1}^{\infty} \xi_{ij} \gamma_j \quad (2.5)$$

and approximate  $h(y|\mathbf{x}_i, Z_i(\cdot))$  as

$$h_0(y) \exp\left(\sum_{k=1}^p x_{ik} \beta_k + \sum_{j=1}^{\infty} \xi_{ij} \gamma_j\right) \approx h_0(y) \exp\left(\sum_{k=1}^p x_{ik} \beta_k + \sum_{j=1}^{q_n} \xi_{ij} \gamma_j\right), \quad (2.6)$$

where  $q_n$  is a sufficiently large integer that may depend on  $n$ . As shown in the literature, such an approximation is accurate under some conditions on the decay rate of the  $\gamma_j$ 's. Practically, it is common to choose  $q_n$  such that the percentage of variance explained by the first  $q_n$  fPCA components is 70%, 85%, or 95%. Alternatively, we may formulate it as a

model selection procedure and choose it by using some model selection criterion, such as the deviance information criterion (DIC) [34, 71].

### 2.3. Priors

To carry out a Bayesian analysis of model (2.6), we specify joint prior distributions for all unknown parameters  $(\beta, \gamma, h_0)$ , where  $h_0(\cdot)$  is the baseline hazard function. We first set  $p(\beta, \gamma, h_0) = p(\beta, \gamma)p(h_0)$  and assume  $(\beta, \gamma) \sim N(\mu_0, \Sigma_0)$ , where  $N(\mu_0, \Sigma_0)$  is the multivariate Normal distribution with  $s(p + q_n) \times 1$  mean vector  $\mu_0$  and a  $(p + q_n) \times (p + q_n)$  covariance matrix  $\Sigma_0$ .

We may specify different prior distributions for  $h_0(y)$ . The most convenient and popular distribution for  $h_0(y)$  is the piecewise constant hazard model. Specifically, we first construct a finite partition of the time axis,  $0 < s_1 < s_2 < \dots < s_J$ , with  $s_J > y_i$  for all  $i$ , which leads to  $J$  intervals  $(0, s_1], \dots, (s_{J-1}, s_J]$ . In the  $j$ -th interval, we set  $h_0(y) = \lambda_j$  for  $y \in I_j = (s_{j-1}, s_j]$ . A common prior of the baseline hazard  $\lambda = (\lambda_1, \dots, \lambda_J)^T$  is the independent gamma prior  $\lambda_j \sim \mathcal{G}(\alpha_{0j}, \alpha_{1j})$  for  $j = 1, \dots, J$ , where  $\alpha_{0j}$  and  $\alpha_{1j}$  are prior hyperparameters. Another approach is to build prior correlation among the  $\lambda_j$ 's using a prior  $\psi \sim N(\psi_0, \Sigma_\psi)$ , where  $\psi_j = \log(\lambda_j)$  for  $j = 1, \dots, J$  and  $\psi_j = (\psi_1, \dots, \psi_J)$ . For notational simplicity, we focus on the piecewise constant hazard model with the independent gamma prior from here on.

We consider the strategy of choosing the hyperparameters  $\Sigma_0$ ,  $\alpha_{0j}$  and  $\alpha_{1j}$  as follows. We can tune the eigenvalues of  $\Sigma_0$  in order to control the prior information for the regression coefficients. If the smallest eigenvalue  $\lambda_{\min}(\Sigma_0)$  converges to  $\infty$ , then  $N(\mu_0, \Sigma_0)$  tends to be an improper prior. In contrast, if the largest eigenvalue  $\lambda_{\max}(\Sigma_0)$  is very small, then  $N(\mu_0, \Sigma_0)$  tends to be a strongly informative prior. In order to use a noninformative prior for the  $\lambda_j$ 's, the shape and scale parameters of the gamma distributions are set to be  $\alpha_{0j} = 0.2$  and  $\alpha_{1j} = 0.4$  for all  $j = 1, \dots, J$  [69]. Also setting either  $(\alpha_{0j}, \alpha_{1j}) = (0.5, 1)$  or  $(\alpha_{0j}, \alpha_{1j}) = (0.2, 1)$  would make the gamma distribution flat as well.

### 2.4. Posterior Computation

The log-posterior distribution of  $(\beta, \gamma, \lambda)$  (unnormalized) is given by

$$\sum_{i=1}^n \sum_{j=1}^J \left[ u_{ij} \nu_i \left( \log \lambda_j + z_i^T \theta \right) - u_{ij} \left\{ \lambda_j (y_i - s_{j-1}) + \sum_{g=1}^{j-1} \lambda_g (s_g - s_{g-1}) \right\} \exp \left( z_i^T \theta \right) \right] - \left\{ \log |\Sigma_0| + (\theta - \mu_0)^T \Sigma_0^{-1} (\theta - \mu_0) \right\} / 2 + \sum_{j=1}^J \{ (\alpha_{0j} - 1) \log \lambda_j - \lambda_j \alpha_{1j} + \alpha_{0j} \log (\alpha_{1j}) - \log \Gamma (\alpha_{0j}) \}, \tag{2.7}$$

where  $\theta = (\beta^T, \gamma^T)^T$ ,  $z_i = (x_i^T, \xi_{i1}, \dots, \xi_{iq_n})^T$ , and  $s_0 = 0$ . Moreover,  $u_{ij} = 1$  if the  $i$ -th subject is right censored in the  $j$ -th interval and 0 otherwise. We propose a Gibbs sampler for posterior computation after truncating the sum of the infinite series to have  $q_n < \infty$  terms. The Gibbs sampler is computationally efficient and mixes rapidly. We first specify the hyperparameters  $\mu_0$ ,  $\Sigma_0$ ,  $\alpha_{0j}$  and  $\alpha_{1j}$  for all  $j$  at appropriate values to represent prior

opinion. Starting from the initiation step, the Gibbs sampler for model (2.6) with the truncated term  $q_n$  proceeds as follows:

1. Update  $(\beta, \gamma)$  according to their full conditional distribution in (2.7). Specifically, we employ the random walk Metropolis-Hastings (M-H) [31, 47] algorithm and choose a multivariate Normal proposal density yielding an average acceptance rate of 23.4% [27]. The mean of the proposal density is the posterior sample  $(\beta^{-1}, \gamma^{-1})$  from the previous iteration. The covariance matrix is the inverse of the Fisher information matrix of the posterior distribution evaluated at  $(\beta^{-1}, \gamma^{-1})$ .
2. Update  $\lambda_j$  from its full conditional distribution

$$p(\lambda_j | \lambda_0^{(-j)}, -) \sim \text{Gamma}\left(\alpha_{0j} + \sum_{i=1}^n u_{ij} \nu_i, \tilde{\alpha}_{1j}\right),$$

where  $\lambda_0^{(-j)}$  is the vector  $\lambda_0$  without the  $j$ -th element and  $\tilde{\alpha}_{1j}$  is given by

$$\tilde{\alpha}_{1j} = \begin{cases} \alpha_{1j} + \sum_{i=1}^n \left\{ u_{ij} (y_i - s_{j-1}) + (s_j - s_{j-1}) \sum_{k=j+1}^J u_{ik} \right\} \exp(z_i^T \theta), & \text{if } j \leq J-1; \\ \alpha_{1j} + \sum_{i=1}^n \left\{ u_{ij} (y_i - s_{j-1}) \exp(z_i^T \theta) \right\}, & \text{if } j=J. \end{cases}$$

### 3. Alzheimer’s Disease Neuroimaging Initiative Data Analysis

#### 3.1. Alzheimer’s Disease Neuroimaging Initiative

The development of the BFLCRM is motivated by the analysis of imaging, genetic, and clinical data collected by ADNI. “Data used in the preparation of this article were obtained from the Alzheimers Disease Neuroimaging Initiative (ADNI) database ([www.loni.usc.edu/ADNI](http://www.loni.usc.edu/ADNI)). The ADNI was launched in 2003 by the National Institute on Aging (NIA), the National Institute of Biomedical Imaging and Bioengineering (NIBIB), the Food and Drug Administration (FDA), private pharmaceutical companies and non-profit organizations, as a \$60 million, 5-year public private partnership. The primary goal of ADNI has been to test whether serial magnetic resonance imaging (MRI), positron emission tomography (PET), other biological markers, and clinical and neuropsychological assessment can be combined to measure the progression of mild cognitive impairment (aMCI) and early Alzheimers disease (AD). Determination of sensitive and specific markers of very early AD progression is intended to aid researchers and clinicians to develop new treatments and monitor their effectiveness, as well as lessen the time and cost of clinical trials. The Principal Investigator of this initiative is Michael W. Weiner, M.D., VA Medical Center and University of California - San Francisco. ADNI is the result of efforts of many co-investigators from a broad range of academic institutions and private corporations, and subjects have been recruited from over 50 sites across the U.S. and Canada. The initial goal of ADNI was to recruit 800 adults, ages 55 to 90, to participate in the research approximately 200 cognitively normal older individuals to be followed for 3 years, 400 people with aMCI to be followed

for 3 years, and 200 people with early AD to be followed for 2 years. For up-to-date information see [www.adni-info.org](http://www.adni-info.org).”

### 3.2. Data Description

The aim of this ADNI data analysis is to examine the predictability of clinical, genetic, and imaging data for the time to conversion to AD in MCI patients. We focused on 346 MCI patients at baseline of the ADNI-1 database. Among the 346 MCI patients, 151 of them are converters and 195 are non-converters at 48 months.

For each MCI patient, we included his/her clinical, genetic, and imaging variables at baseline. The clinical characteristics include Gender (0=Male; 1=Female), Handedness (0=Right; 1=Left), Marital Status (1=Married; 2=Widowed; 3=Divorced; 4=Never married), Education length, Retirement (1=Yes; 0=No), Age, and Alzheimer’s Disease Assessment Scale-Cognition (ADAS-Cog) score. Marriage status is coded using 3 dummy variables: “Widowed”, “Divorced”, “Never married”. The ADAS-Cog test has been widely used to assess the severity of dysfunction in adults [62]. The genetic variables include the APOE genetic covariates, since it is well known that mutations in APOE raise the risk of progression from amnesic MCI to AD[56]. The Apolipoprotein E (APOE) SNPs, rs429358 and rs7412 were, separately, genotyped in ADNI-1. These two SNPs together define a 3 allele haplotype, namely the  $\epsilon 2$ ,  $\epsilon 3$ , and  $\epsilon 4$  variants and the presence of each of these variants was available in the ADNI database for all the individuals. Among these variants, APOE- $\epsilon 3$  is known to be most common allele, while APOE- $\epsilon 4$  has been turned out to be a risk factor for early onset of AD. [52]. In this model, we consider the presence of APOE- $\epsilon 4$  as a covariate to incorporate its effect on the time to conversion from MCI to AD. In addition, we selected 7 regions of interest (ROIs) which may significantly influence MCI progression among the 93 ROI volume data [6, 22, 37]. These 7 ROIs are bilateral hippocampal formation, bilateral amygdala, posterior limb of internal capsule, bilateral thalamus. In total, we have 17 scalar covariates. The imaging data include the hippocampal radial distances of 30,000 surface points on the left and right hippocampal surfaces. The hippocampal radial distance is a distance from its medial core to the hippocampal surface and measures hippocampal thickness.

In the demographic information, 220 participants are male, and 126 are female; 316 are right-handed, and 30 are left-handed. For Marital Status, 283 were married, 40 were widowed, 19 were divorced, and 4 were never married at baseline. Among these individuals, 276 were retired and 70 were not. On average, the subjects had 15.7 years of education with standard deviation 3.0 years, the minimum 6 years, and the maximum 20 years. The average age of subjects was 75.0 years with standard deviation of 7.3 years. The youngest person was 55 years old, while the oldest person was 90 years old. For the genetics information on the first allele of APOE, 25 subjects had genotype 2, 277 subjects had genotype 3, and 44 subjects had genotype 4. For the second allele, 156 subjects had genotype 3, while 190 subjects had genotype 4. The average ADAS-cog score was 11.5, with standard deviation of 4.4. The lowest score was 2 and the highest score was 27.67.

### 3.3. Hippocampus Image Preprocessing

We used a hippocampal image analysis package to calculate hippocampal surface data as follows [8, 46, 50, 66, 67, 68, 77]. Given the 3D MRI scans, we used FIRST [53] to segment hippocampal substructures and then applied the marching cube method [45] to automatically reconstructing hippocampal surfaces. Then, an automatic algorithm, called topology optimization, was used to introduce two cuts on a hippocampal surface in order to convert it into a genus zero surface with two open boundaries. The two cuts, whose locations were at the front and back of the hippocampal surface, represent its anterior junction with the amygdala and its posterior limit as it turns into the white matter of the fornix. We then computed holomorphic 1-form basis functions [76]. It allows us to induce conformal grids of the hippocampal surfaces which were consistent across subjects. The conformal representation of the surface was computed with this conformal grid [66]. We also computed the “feature image” of a surface by combining the conformal factor and mean curvature and linearly scaling the dynamic range into [0, 255]. Finally, the feature image of each surface in the dataset was registered to a common template by using an inverse consistent fluid registration algorithm [68]. It establishes high-order correspondences between 3D surfaces. Finally, we computed various surface statistics based on the registered surface, such as multivariate tensor-based morphometry (mTBM) statistics [76].

### 3.4. Data Analysis

We focused on 346 MCI patients in the ADNI-1 data in order to examine the predictability of clinical, genetic, and imaging covariates for the time to conversion to AD from MCI. The patients consist of 151 converters and 195 non-converters. We fit BFLCRM with time to conversion to AD as the response  $y_i$ , the clinical, genetic, and ROI volume data as scalar covariates in  $x_i$ , and the hippocampus surface data based on radial distance as functional covariates in  $Z_i(\cdot)$  for the  $i$ -th subject. In all posterior computations, we centered the scalar covariates  $x_i$  using their mean. We chose the first 14 eigenfunctions of hippocampal surface data, which explain about 73.48% of the variance in the hippocampus surface data. The first 14 largest eigenfunctions projected on the hippocampal surfaces were presented in Figure 3 in the supplementary document. For the piecewise constant hazards model of  $h_0(\cdot)$ , we chose  $J = 70$  intervals so that each interval contains at least one failure or censored observation. The full BFLCRM model (2.6) contains 19 scalar covariates and the first 14 fPC scores.

Due to the lack of prior information, all hyperparameters were chosen to reflect nearly noninformative priors. For regression coefficients, the hyperparameters of the multivariate Normal priors were set as  $\mu_0 = (0, \dots, 0)$  and  $\Sigma_0 = \text{diag}(5, \dots, 5)$ . For the  $\gamma_j$ 's, the shape and scale parameters of the Gamma priors were set to be  $\alpha_{0j} = 0.2$  and  $\alpha_{1j} = 0.4$  for  $j = 1, \dots, 70$  [69]. We ran the Gibbs sampler for 25,000 iterations after 5,000 burn-in iterations. Based on the 20,000 MCMC samples, we calculated various posterior quantities of  $(\beta, \gamma, \lambda)$ . For the full BFLCRM model, we also conducted sensitivity analyses in order to investigate the influence of different choices of hyperparameters in the prior distributions. From the results shown in Tables 1 and 2 in the supplementary document, we found that the proposed priors were robust to various choices of the hyperparameters in the prior distributions. The computational time (in C/C++ using an 8-cores 2.80 GHz Intel processors) was 350 seconds for running the Gibbs sampler for the full BFLCRM model with 25,000 iterations.

Table 1 shows the posterior means of the regression coefficients  $\beta$  and their standard deviations, as well as the lower and upper limits of the 95% highest posterior density (HPD) intervals based on the full BFLCRM model. Six scalar covariates including “Length of Education”, “Age”, “APOE- $\epsilon 4$  carrier”, “ADAS-cog score”, “Left Hippocampal formation”, and “Right amygdala” have 95% HPD intervals that do not contain 0. This implies that we can expect a worse prognosis of AD for MCI patients with lower ROI volume in the left hippocampal formation and the right amygdala. This finding supports the finding that atrophy of the hippocampal formation is a significant diagnostic marker [35, 42]. It also confirms the previous finding that the amygdala volume tends to be reduced in the early stage of AD [49, 57]. Moreover, the 95% HPD intervals of the 1st, 7th, and 14th fPCs do not contain 0. This may indicate that the hippocampal radial distance is an important functional covariate for predicting the time to conversion to AD in MCI subjects.

We estimated the coefficient function  $\gamma(\cdot)$  by using  $\hat{\gamma}(s) = \sum_{j=1}^{14} \hat{\phi}_j(s) \hat{\gamma}_j$ , where  $\hat{\gamma}_j$  is the posterior mean of  $\gamma_j$  for each  $j$ . Figure 4 shows the estimated coefficient function  $\hat{\gamma}(\cdot)$  associated with the hippocampal surface data. When hippocampal atrophy in a red region is greater, a risk of progressing from MCI to AD is expected to be increased. A blue region suggests that the thicker the area is on the hippocampus, the shorter the time to conversion to AD is. Inspecting Figure 4 reveals that the subfields of CA1 and subiculum on the hippocampi have positive effects on the hazard function, indicating that the thinner these areas on the hippocampus are, the shorter the time is to conversion to AD.

Figure 3 shows the estimated survival functions of the APOE- $\epsilon 4$  carriers and non-carriers, when the values of the continuous covariates are set at their mean values and the categorical variables are set at their reference levels. The dotted lines show the 95% HPD intervals of survival functions. The APOE- $\epsilon 4$  carriers are expected to convert from MCI to AD faster than non-carriers. These results are consistent with several prior studies suggesting that the presence of the APOE- $\epsilon 4$  allele increases the risk of developing AD [9, 63, 72].

We compared the full BFLCRM model with three reduced models in terms of their predictive performance. For Model 1, we excluded the ROI volume covariates from the full BFLCRM model. For Model 2, we only included all the scalar covariates. For Model 3, we only included the clinical covariates, APOE- $\epsilon 4$  status, and the ADAS-cog score. For all three reduced models, we set  $J = 70$  intervals so that each interval contains at least one failure or censored observation. For the regression coefficients, the hyperparameters of the multivariate Normal priors were set as  $\mu_0 = (0, \dots, 0)$  and  $\Sigma_0 = \text{diag}(5, \dots, 5)$ . We set  $\alpha_{0j} = 0.2$  and  $\alpha_{1j} = 0.4$  for  $j = 1, \dots, 70$ . We ran the Gibbs sampler for 25,000 iterations after 5,000 burn-in iterations. We also calculated the Deviance Information Criterion (DIC) and integrated AUC (iAUC) for all four models, where AUC denotes the area under the Receiver Operating Characteristic (ROC) curve. The DIC can be estimated within the MCMC iterations. More details can be found in [34, 71].

Table 2 shows the values of DIC and iAUC for the four models. The full BFLCRM model yields the DIC value of 427.19, which is smaller than those of Models 3, but larger than those of Model 1 and 2. The Model 1 had the smallest DIC value as 413.08. For Model 1, as

shown in Table 3, “Age”, “APOE-ε4 carrier”, and “ADAS-cog score” have their 95% HPD intervals that do not contain 0. See additional estimation results associated with Models 1-3 in Tables 3-4 and Figures 1 and 2 of the supplementary document. Based on the iAUC values, however, the full BFLCRM model achieves the best predictive performance. Moreover, the full model and Model 1, that include the hippocampal surface data as functional covariates, provide better predictive performance than Models 2 and 3. This may indicate that the hippocampal surface data contributes significantly to the time of conversion from MCI to AD. We estimated the iAUC by using a Monte Carlo cross-validation (MCCV) method [32]. Specifically, the full data set was randomly split into a training set with 200 subjects and a test set with 146 subjects. For each such split, we fitted each model to the training set and then calculated iAUC based on the test set. This random split was repeated 100 times yielding the estimated iAUC values for all models.

#### 4. Simulation Studies

We conduct Monte Carlo simulations to evaluate the proposed BFLCRM across different censoring rates and sample sizes. Moreover, we will evaluate the predictability of our BFLCRM compared to proportional hazards models without the use of functional covariates.

##### 4.1. Setup

We generated all simulated data sets according to model (2.1). The  $\mathbf{x}_i$  is a  $4 \times 1$  vector and its corresponding elements were independently generated from  $N(0, 0.5)$ . We set the true value of  $\beta$  to be  $(0.7, 0.2, -0.5, -1)^T$ . The functional covariate  $Z_i(s)$  was generated from model (2.3), where its underlying function follows the standard Gaussian process with the covariance function  $K(s, t) = \exp(-3(s - t)^2)$ . The observed functional covariate data  $W_i(s)$  consists of noisy observations evaluated at 100 equally spaced grids in the interval  $[-4, 4]$  with some measurement errors. Specifically, the measurement errors  $\epsilon_i(s)$  were independently generated from a  $N(0, 0.5)$  across  $s$ . The functional coefficient  $\gamma(s)$  was generated from the standard Gaussian process with covariance function  $K_\gamma(s, t) = \exp(-2(s - t)^2)$ . To generate the survival time, we considered two different baseline hazard functions  $h_{01}(\cdot)$  and  $h_{02}(\cdot)$  as follows.

$$h_{01}(t) = 1 \text{ if } t > 0, \quad (4.1)$$

$$h_{02}(t) = \begin{cases} \kappa\omega & \text{if } 0 < t \leq 2; \\ \kappa\omega(t - 1)^{\omega-1} & \text{if } 2 < t \leq 3; \\ \kappa\omega 2^{\omega-1} & \text{if } t > 3. \end{cases} \quad (4.2)$$

The first baseline hazard function  $h_{01}(\cdot)$  assumes that it is constant over time. As a more general form of hazard function, we consider a mixed form of baseline hazard functions for the exponential and Weibull distributions. The hazard function  $h_{02}(\cdot)$  depends on  $\kappa$  and  $\omega$ . In this simulation study, we set  $\kappa = 1/3$  and  $\omega = 2$ . Finally, the censoring times were independently generated from a uniform distribution with parameter chosen to achieve a

desired censoring rate of 30% or 50%. We considered sample sizes of  $n = 200$  and  $n = 500$  for each censoring rate and simulated 100 data sets for each case.

#### 4.2. Simulation Results

We used the piecewise constant hazard model for  $h_0(s)$ , in which we set  $J = 5$  and subintervals  $(s_{j-1}, s_j]$  to be of equal length. We set  $(a_{0j}, a_{1j}) = (0.2, 0.4)$  for all  $j$ ,  $\Sigma_0 = \text{diag}(5, \dots, 5)$ , and  $\mu_0 = \text{diag}(0, \dots, 0)^T$ . We calculated the first 12 fPC scores explaining 95% of the variation of the functional covariates, and then compared the estimation results using the first 12 PC scores in order to investigate the efficacy of using fPCA. For each simulated data set, we ran the Gibbs sampler for 20,000 iterations with 5,000 burn-in iterations.

To examine the estimation and prediction performance of BFLCRM, we calculated mean squared errors (MSEs) and time-dependent integrated area under the curve (iAUC)[32] based on 100 simulated data sets for each scenario. The computational time (in C/C++ using an 8-cores 2.80 GHz Intel processor) was 50.3 seconds for BFLCRM with sample size 200 for one repetition. We let  $\hat{\beta}$  denote the posterior mean of  $\beta$ . The MSE of  $\hat{\beta}$  is defined by

$$MSE_{\hat{\beta}} = \sum_{j=1}^p (\hat{\beta}_j - \beta)^2, \text{ whereas the MSE for } \gamma(\cdot) \text{ is defined by}$$

$MSE_{\hat{\gamma}} = \int_{-4}^4 \{\hat{\gamma}(s) - \gamma(s)\}^2 ds$ , where  $\hat{\gamma}(s)$  denotes the posterior mean of  $\gamma$  at time  $s$ . A smaller MSE implies better estimation accuracy, and a large value of iAUC implies a better predictive model. To evaluate the predictive value of the functional covariate to the hazard function, we calculated iAUC for two nested models including a reduced BFLCRM model with solely scalar covariates in  $\mathbf{x}_i$  and a full BFLCRM model with both  $W_i(\cdot)$  and  $\mathbf{x}_i$ .

Table 4 presents the estimation results with  $h_{01}(\cdot)$  in (4.1) based on 100 simulated data sets for each scenario. The MSE values of both  $\hat{\beta}$  and  $\hat{\gamma}(\cdot)$  are fairly small in all the cases. The values of iAUC indicate reasonable predictive performance of our BFLCRM. The MSE value decreases as either the sample size gets larger or the censoring rate gets smaller. Also, estimation results of fPCA are better than those of PCA in both MSE and iAUC. When the functional covariate has moderate measurement noise, fPCA will lead better estimation and prediction results since the use of smoothing step in fPCA can dramatically reduce measurement errors. Table 5 presents the means and standard errors of iAUC for the reduced and full BFLCRM models under each scenario. The iAUC value of the full BFLCRM model is generally larger than that of the reduced model in all scenarios. This may indicate that the use of functional covariates can improve predictability of the hazard function. Figure 5 shows the baseline hazard functions estimated by the full BFLCRM from the first 10 data sets in the sample size 500 cases. The dotted lines show the estimated baseline hazard functions, and the true baseline hazard function  $h_{01}(\cdot)$  is plotted as a solid line on each plot. When the true baseline hazard function is constant, our model estimates the true function well in low to moderate censoring cases.

Table 6 presents the estimation results with  $h_{02}(\cdot)$  in (4.1) based on 100 simulated data sets for each scenario. Table 7 shows iAUC values for the two nested models. These results in Tables 6 and 7 are consistent with those based on  $h_{01}(\cdot)$ . The estimated baseline hazard

functions are presented in Figure 6 for the sample size 500 cases. We plot the estimated baseline hazard functions of the first 10 data sets using the full BFLCRM model. The solid line shows the true baseline hazard function  $h_{02}(\cdot)$  on each plot. When the true baseline hazard function is not piecewise constant, it is well approximated by the estimated baseline hazard function in the low censoring case. In the moderate censoring case, our model captures the general pattern of the true baseline hazard function. It may indicate that our BFLCRM approximates the general form of the baseline hazard function fairly well and therefore it is applicable for most of the practical settings.

## 5. Discussion

The BFLCRM was developed to predict the time of conversion from MCI to AD, as well as to determine the optimal set of predictors at baseline that effect the time of conversion. We obtained estimation and prediction results for functional and scalar predictors. This study has examined a very large set of predictors for predicting the time of conversion from MCI to AD. We observed several important predictors including (i) gender, (ii) handedness, (iii) APOE status, and (iv) surface morphology changes with the right and left hippocampi. These findings highlight the importance of including not only demographic and clinical information, but also high-dimensional imaging data, in statistical analyses of MCI-AD conversion. These results are also consistent with newly published clinical research criteria which incorporate the use of an array of biomarkers in research settings and clinical trials [1].

Several prior studies have highlighted the importance of hippocampal changes in the context of AD-related neurodegeneration and prediction of MCI-AD conversion [18]. These studies, however, commonly assess changes to hippocampal volume rather than surface morphology. The current analysis includes both measures of volume and surface area, with the changes in surface morphology adding additional predictive value.

As shown in Figure 4, the changes in surface area occur more prominently on the anterior portion of the long axis of the hippocampus. Functional MRI studies in healthy adults suggest that anterior portions of the hippocampus are critical for the mnemonic binding processes that are engaged in tasks of episodic (day-to-day) memory. Since episodic memory tasks, particularly those that require binding operations, are some of the earliest cognitive impairments observed in MCI-AD [2], the anterior surface changes identified in the current analysis may underlie these early memory changes and serve as an important predictor of time of conversion.

From Figure 4, we observed that when hippocampal atrophy was greater in the CA1 subfield and subiculum of the hippocampi, it took shorter to progress to AD. Similar to our finding, it was reported that greater atrophy of CA1 and subicular subfields in hippocampi was related to increased risk for conversion from MCI to AD [3]. The subregional atrophy rate in the CA1 and subicular subfields was also turned out to be the best predictor to explain the progression to AD from MCI [25]. Also, it was revealed that left hippocampal body volume was associated with delayed verbal memory [7], where the delayed verbal memory was one

of important predictor for determining whether a subject was a MCI converter or not [28]. Thus, our finding in Figure 4 supports these research results.

Beyond the important effects on hippocampal surface morphology, we observed important volumetric changes in the left hippocampal formation and the right amygdala. There has been extensive research to diagnose Alzheimer's disease by using atrophy of various brain regions [15, 17, 36,64]. In particular, it was reported that the volume hippocampal formation showed significant reduction in patients with clinically diagnosed Alzheimer's disease [35, 42]. It was also found that the amygdala volume was reduced in very early AD, which suggested that MRI-based amygdaloid volumetric measurement was a relevant biomarker [49]. Also, as shown in [57], the level of amygdala atrophy is related to global illness severity in the early stage of AD. Our ADNI-1 data analysis results agree with these findings in that volumetric changes in the hippocampal formation is an important variable to predict the time to conversion from MCI to AD.

The analysis also shows that APOE status exerts important effects on the time of conversion. Our results also agree with several prior studies that have documented that the presence of the APOE  $\epsilon 4$  allele increases the risk of developing Alzheimer's disease. Particularly, if a subject has APOE  $\epsilon 4$ , then MCI progression more likely occurs.

We have demonstrated the utility of BFLCRM as a valuable method for identifying optimal early markers of conversion to AD in patients with MCI. The early markers identified from our analysis could be used in case selection for various clinical trials for evaluating drug/therapeutic efficiency in slowing or modifying AD-related pathophysiology, when such drugs and therapeutic treatments are available.

There are some limitations to our analysis. Our findings survived internal cross validation, but they need replication in an independent community-based sample. We did not include measures of pathology (e.g. beta-amyloid) in our models since CSF and amyloid-PET were available only in a small subset of individuals in ADNI-1. However, a study of ADNI-2 subjects has shown a robust correlation between the APOE  $\epsilon 4$  allele and cortical amyloid burden [51], suggesting that APOE  $\epsilon 4$  may have served as a surrogate for cortical amyloid plaque load in our analysis.

We have developed BFLCRM for the use of functional and scalar covariates to predict time-to-event outcomes. Several important methodological issues need to be addressed in future research. First, it would be interesting to investigate the theoretical properties of our Bayesian procedure, including the support of the prior and truncation approximation bounds  $q_n$ . Second, it is interesting to develop a new Bayesian method to automatically determine the distribution of  $q_n$ . Third, it is interesting to incorporate high-dimensional scalar covariates (e.g., genetic markers in the whole genome) in FLCRM and develop its associated estimation and testing procedures. Developing such statistical methods poses many new challenges both computationally and theoretically.

## Supplementary Material

Refer to Web version on PubMed Central for supplementary material.

## Acknowledgements

We thank the Editor Professor Beth Ann Griffin, the Associate Editor and two anonymous referees for valuable suggestions, which have greatly helped to improve our presentation.

## References

- [1]. Albert MS, DeKosky ST, Dickson D, Dubois B, Feldman HH, Fox NC, Gamst A, Holtzman DM, Jagust WJ, Petersen RC, Snyder PJ, Carrillo MC, Thies B, Phelps CH. The diagnosis of mild cognitive impairment due to Alzheimer's disease: Recommendations from the National Institute on Aging-Alzheimer's Association workgroups on diagnostic guidelines for Alzheimer's disease. *Alzheimer's & Dementia*. 2011; 7:270–279.
- [2]. Anderson ND, Ebert PL, Jennings JM, Grady CL, Cabeza R, Graham SJ. Recollection-and familiarity-based memory in healthy aging and amnesic mild cognitive impairment. *Neuropsychology*. 2008; 22:177–187. [PubMed: 18331160]
- [3]. Apostolova LG, Dutton RA, Dinov ID, Hayashi KM, Toga AW, Cummings JL, Thompson PM. Conversion of mild cognitive impairment to Alzheimer disease predicted by hippocampal atrophy maps. *Archives of neurology*. 2006a; 63:693–699. [PubMed: 16682538]
- [4]. Apostolova LG, Dinov ID, Dutton RA, Hayashi KM, Toga AW, Cummings JL, Thompson PM. 3D comparison of hippocampal atrophy in amnesic mild cognitive impairment and Alzheimer's disease. *Brain*. 2006b; 129:2867–2873. [PubMed: 17018552]
- [5]. Biswas, A.; Datta, S.; Fine, JP.; Segal, MR. *Statistical Advances in the Biomedical Sciences: Clinical Trials, Epidemiology, Survival analysis, and Bioinformatics*. Vol. 630. John Wiley & Sons; 2007.
- [6]. Bryant C, Giovanello KS, Ibrahim JG, Chang J, Shen D, Peterson BS, Zhu H, ADNI. Mapping the genetic variation of regional brain volumes as explained by all common SNPs from the ADNI study. *PLoS One*. 2013; 8:e71723. [PubMed: 24015190]
- [7]. Chen KH, Chuah LY, Sim SK, Chee MW. Hippocampal region-specific contributions to memory performance in normal elderly. *Brain and Cognition*. 2010; 72:400–407. [PubMed: 20044193]
- [8]. Colom R, Stein JL, Rajagopalan P, Martínez K, Hermel D, Wang Y, Álvarez-Linera J, Burgaleta M, Quiroga M, Shih PC, Thompson PM. Hippocampal structure and human cognition: Key role of spatial processing and evidence supporting the efficiency hypothesis in females. *Intelligence*. 2013; 41:129–140. [PubMed: 25632167]
- [9]. Corder E, Saunders A, Strittmatter W, Schmechel D, Gaskell P, Small G, Roses A, Haines J, Pericak-Vance MA. Gene dose of apolipoprotein E type 4 allele and the risk of Alzheimer's disease in late onset families. *Science*. 1993; 261:921–923. [PubMed: 8346443]
- [10]. Costafreda SG, Dinov ID, Tu Z, Shi Y, Liu CY, Kloszewska I, Mecocci P, Soininen H, Tsolaki M, Vellas B, Wahlund LO, Spenger C, Toga AW, Lovestone S, Simmons A. Automated hippocampal shape analysis predicts the onset of dementia in mild cognitive impairment. *Neuroimage*. 2011; 56:212–219. [PubMed: 21272654]
- [11]. Cox DR, et al. Regression models and life tables. *Journal of Royal Statistical Society. Series B*. 1972; 34:187–220.
- [12]. Cui Y, Liu B, Luo S, Zhen X, Fan M, Liu T, Zhu W, Park M, Jiang T, Jin JS, ADNI. Identification of conversion from mild cognitive impairment to Alzheimer's disease using multivariate predictors. *PLoS One*. 2011; 6:e21896. [PubMed: 21814561]
- [13]. Da X, Toledo JB, Zee J, Wolk DA, Xie SX, Ou Y, Shacklett A, Parmpi P, Shaw L, Trojanowski JQ, Davatzikos C. Integration and relative value of biomarkers for prediction of MCI to AD progression: spatial patterns of brain atrophy, cognitive scores, APOE genotype, and CSF markers. *Neuroimage: Clinical*. 2014; 4:164–173. [PubMed: 24371799]
- [14]. de la Torre JC. Alzheimer's disease is incurable but preventable. *Journal of Alzheimer's Disease*. 2010; 20:861–870.
- [15]. De Leon M, George A, Golomb J, Tarshish C, Convit A, Kluger A, De Santi S, Mc Rae T, Ferris S, Reisberg B, et al. Frequency of hippocampal formation atrophy in normal aging and Alzheimer's disease. *Neurobiology of Aging*. 1997; 18:1–11. [PubMed: 8983027]

- [16]. Desikan RS, Cabral HJ, Fischl B, Guttman CRG, Blacker D, Hyman BT, Albert MS, Killiany RJ. Temporoparietal MR imaging measures of atrophy in subjects with mild cognitive impairment that predict subsequent diagnosis of Alzheimer disease. *American Journal of Neuroradiology*. 2009; 30:532–538. [PubMed: 19112067]
- [17]. Devanand D, Pradhaban G, Liu X, Khandji A, De Santi S, Segal S, Rusinek H, Pelton G, Honig L, Mayeux R, et al. Hippocampal and entorhinal atrophy in mild cognitive impairment prediction of Alzheimer disease. *Neurology*. 2007; 68:828–836. [PubMed: 17353470]
- [18]. Dickerson BC, Wolk DA, ADNI. Biomarker-based prediction of progression in MCI: comparison of AD signature and hippocampal volume with spinal fluid amyloid- $\beta$  and tau. *Frontiers in Aging Neuroscience*. 2013; 5
- [19]. Dickerson BC, Goncharova I, Sullivan MP, Forchetti C, Wilson RS, Bennett DA, Beckett LA, deToledo Morrell L. MRI-derived entorhinal and hippocampal atrophy in incipient and very mild Alzheimer's disease. *Neurobiology of Aging*. 2001; 22:747–754. [PubMed: 11705634]
- [20]. Fan J, Lv J. A selective overview of variable selection in high dimensional feature space. *Statistica Sinica*. 2010; 20:101–148. [PubMed: 21572976]
- [21]. Fan Y, Batmanghelich N, Clark CM, Davatzikos C. Spatial patterns of brain atrophy in MCI patients, identified via high-dimensional pattern classification, predict subsequent cognitive decline. *Neuroimage*. 2008; 39:1731–1743. [PubMed: 18053747]
- [22]. Fennema-Notestine C, Hagler DJ, McEvoy LK, Fleisher AS, Wu EH, Karow DS, Dale AM. Structural MRI biomarkers for preclinical and mild Alzheimer's disease. *Human Brain Mapping*. 2009; 30:3238–3253. [PubMed: 19277975]
- [23]. Ferraty, F.; Vieu, P. *Nonparametric Functional Data Analysis: Methods, Theory, Applications and Implementation*. Springer; New York: 2006.
- [24]. Fleming, TR.; Harrington, DP. *Counting processes and survival analysis*. Vol. 169. John Wiley & Sons; 2011.
- [25]. Frankó E, Joly O, Initiative ADN, et al. Evaluating Alzheimers disease progression using rate of regional hippocampal atrophy. *PloS one*. 2013; 8:e71354. [PubMed: 23951142]
- [26]. Gauthier S, Reisberg B, Zaudig M, Petersen RC, Ritchie K, Broich K, Belleville S, Brodaty H, Bennett D, Chertkow H, Cummings JL, de Leon M, Feldman H, Ganguli M, Hampel H, Scheltens P, Tierney MC, Whitehouse P, Winblad B. Mild cognitive impairment. *The Lancet*. 2006; 367:1262–1270.
- [27]. Gelman A, Gilks WR, Roberts GO. Weak convergence and optimal scaling of random walk Metropolis algorithms. *The Annals of Applied Probability*. 1997; 7:110–120.
- [28]. Gomar JJ, Bobes-Bascaran MT, Conejero-Goldberg C, Davies P, Goldberg TE, Initiative ADN, et al. Utility of combinations of biomarkers, cognitive markers, and risk factors to predict conversion from mild cognitive impairment to Alzheimer disease in patients in the Alzheimer's disease neuroimaging initiative. *Archives of General Psychiatry*. 2011; 68:961–969. [PubMed: 21893661]
- [29]. Grundman M, Sencakova D, Jack CR, Petersen RC, Kim HT, Schultz A, Weiner MF, DeCarli C, DeKosky ST, van Dyck C, Thomas RG, Thal LJ, ADCS. Brain MRI hippocampal volume and prediction of clinical status in a mild cognitive impairment trial. *Journal of Molecular Neuroscience*. 2002; 19:23–27. [PubMed: 12212787]
- [30]. Hastie, TJ.; Tibshirani, RJ. *Generalized additive models*. Vol. 43. CRC Press; 1990.
- [31]. Hastings WK. Monte Carlo sampling methods using Markov chains and their applications. *Biometrika*. 1970; 57:97–109.
- [32]. Hung H, Chiang C-T. Estimation methods for time-dependent AUC models with survival data. *Canadian Journal of Statistics*. 2010; 38:8–26.
- [33]. Ibrahim, JG.; Chen, M-H.; Sinha, D. *Bayesian Survival Analysis*. Wiley Online Library; 2005.
- [34]. Ibrahim JG, Chen MH, Kim S. Bayesian variable selection for the Cox regression model with missing covariates. *Lifetime Data Analysis*. 2008; 14:496–520. [PubMed: 18836829]
- [35]. Jack CR, Petersen RC, O'Brien PC, Tangalos EG. MR-based hippocampal volumetry in the diagnosis of Alzheimer's disease. *Neurology*. 1992; 42:183–183. [PubMed: 1734300]

- [36]. Jack CR, Petersen RC, Xu YC, Waring SC, O'Brien PC, Tangalos EG, Smith GE, Ivnik RJ, Kokmen E. Medial temporal atrophy on MRI in normal aging and very mild Alzheimer's disease. *Neurology*. 1997; 49:786–794. [PubMed: 9305341]
- [37]. Jack CR Jr, Knopman DS, Jagust WJ, Shaw LM, Aisen PS, Weiner MW, Petersen RC, Trojanowski JQ. Hypothetical model of dynamic biomarkers of the Alzheimer's pathological cascade. *The Lancet Neurology*. 2010; 9:119–128. [PubMed: 20083042]
- [38]. James G. Generalized linear models with functional predictors. *Journal of Royal Statistical Society. Series B*. 2002; 64:411–432.
- [39]. Huang J, Sun T, Ying Z, Y Y, Zhang C. Oracle inequalities for the lasso in the Cox model. *Ann. Statist.* 2013; 41:1142–1165.
- [40]. Kalbfleisch, JD.; Prentice, RL. *The Statistical Analysis of Failure Time Data*. John Wiley & Sons; 2002.
- [41]. Kaye JA, Moore MM, Dame A, Quinn J, Camicioli R, Howieson D, Corbridge E, Care B, Nesbit G, Sexton G. Asynchronous regional brain volume losses in presymptomatic to moderate AD. *Journal of Alzheimer's Disease*. 2005; 8:51–56.
- [42]. Kesslak JP, Nalcioglu O, Cotman CW. Quantification of magnetic resonance scans for hippocampal and parahippocampal atrophy in Alzheimer's disease. *Neurology*. 1991; 41:51–54. [PubMed: 1985296]
- [43]. Li, J.; Ma, S. *Survival Analysis in Medicine and Genetics*. Chapman & Hall/CRC; 2013.
- [44]. Li S, Okonkwo O, Albert M, Wang MC. Variation in Variables that Predict Progression from MCI to AD Dementia over Duration of Follow-up. *American Journal of Alzheimer's Disease*. 2013; 1:12–28.
- [45]. Lorensen, WE.; Cline, HE. *ACM Siggraph Computer Graphics*. Vol. 21. ACM; 1987. Marching cubes: A high resolution 3D surface construction algorithm; p. 163-169.
- [46]. Luders E, Thompson PM, Kurth F, Hong JY, Phillips OR, Wang Y, Gutman BA, Chou YY, Narr KL, Toga AW. Global and regional alterations of hippocampal anatomy in long-term meditation practitioners. *Human Brain Mapping*. 2013; 34:3369–3375. [PubMed: 22815233]
- [47]. Metropolis N, Rosenbluth AW, Rosenbluth MN, Teller AH, Teller E. Equation of state calculations by fast computing machines. *The Journal of Chemical Physics*. 2004; 21:1087–1092.
- [48]. Misra C, Fan Y, Davatzikos C. Baseline and longitudinal patterns of brain atrophy in MCI patients, and their use in prediction of short-term conversion to AD: results from ADNI. *Neuroimage*. 2009; 44:1415–1422. [PubMed: 19027862]
- [49]. Mizuno K, Wakai M, Takeda A, Sobue G. Medial temporal atrophy and memory impairment in early stage of Alzheimers disease: an MRI volumetric and memory assessment study. *Journal of the neurological sciences*. 2000; 173:18–24. [PubMed: 10675575]
- [50]. Monje M, Thomason ME, Rigolo L, Wang Y, Waber DP, Sallan SE, Golby AJ. Functional and structural differences in the hippocampus associated with memory deficits in adult survivors of acute lymphoblastic leukemia. *Pediatric Blood & Cancer*. 2013; 60:293–300. [PubMed: 22887801]
- [51]. Murphy KR, Landau SM, Choudhury KR, Hostage CA, Shpanskaya KS, Sair HI, Petrella JR, Wong TZ, Doraiswamy PM. Mapping the effects of ApoE4, age and cognitive status on 18F-florbetapir PET measured regional cortical patterns of beta-amyloid density and growth. *Neuroimage*. 2013; 78:474–480. [PubMed: 23624169]
- [52]. Okuizumi K, Onodera O, Tanaka H, Kobayashi H, Tsuji S, Takahashi H, Oyanagi K, Seki K, Tanaka M, Naruse S, et al. ApoE- $\epsilon$ 4 and early-onset Alzheimer's. *Nature genetics*. 1994; 7:10–11. [PubMed: 8075630]
- [53]. Patenaude B, Smith SM, Kennedy DN, Jenkinson M. A Bayesian model of shape and appearance for subcortical brain segmentation. *Neuroimage*. 2011; 56:907–922. [PubMed: 21352927]
- [54]. Pennanen C, Kivipelto M, Tuomainen S, Hartikainen P, Hanninen T, Laakso MP, Hallikainen M, Vanhanen M, Nissinen A, Helkala EL, Vainio P, Vanninen R, Partanen K, Soininen H. Hippocampus and entorhinal cortex in mild cognitive impairment and early AD. *Neurobiology of Aging*. 2004; 25:303–310. [PubMed: 15123335]

- [55]. Perri R, Serra L, Carlesimo GA, Caltagirone C. Amnesic mild cognitive impairment: difference of memory profile in subjects who converted or did not convert to Alzheimer's disease. *Neuropsychology*. 2007; 21:549–558. [PubMed: 17784803]
- [56]. Petersen RC, Thomas RG, Grundman M, Bennett D, Doody R, Ferris S, Galasko D, Jin S, Kaye J, Levey A, Pfeiffer E, Sano M, van Dyck CH, Thal LJ, ADCSG. Vitamin E and donepezil for the treatment of mild cognitive impairment. *New England Journal of Medicine*. 2005; 352:2379–2388. [PubMed: 15829527]
- [57]. Poulin SP, Dautoff R, Morris JC, Barrett LF, Dickerson BC, Initiative ADN, et al. Amygdala atrophy is prominent in early Alzheimer's disease and relates to symptom severity. *Psychiatry Research: Neuroimaging*. 2011; 194:7–13. [PubMed: 21920712]
- [58]. Prestia A, Caroli A, van der Flier WM, Ossenkoppele R, Van Berckel B, Barkhof F, Teunissen CE, Wall AE, Carter SF, Scholl M, Choo IH, Nordberg A, Scheltens P, Frisoni GB. Prediction of dementia in MCI patients based on core diagnostic markers for Alzheimer disease. *Neurology*. 2013; 80:1048–1056. [PubMed: 23390179]
- [59]. Ramsay, JO.; Silverman, BW. *Functional Data Analysis*. Springer-Verlag; New York: 2005.
- [60]. Reiss PT, Ogden RT. Functional generalized linear models with images as predictors. *Biometrics*. 2010; 66:61–69. [PubMed: 19432766]
- [61]. Risacher SL, Saykin AJ, Wes JD, Shen L, Firpi HA, McDonald BC. Baseline MRI predictors of conversion from MCI to probable AD in the ADNI cohort. *Current Alzheimer Research*. 2009; 6:347–361. [PubMed: 19689234]
- [62]. Rosen WG, Mohs RC, Davis KL. A new rating scale for Alzheimer's disease. *The American Journal of Psychiatry*. 1984; 141:1356–1364. [PubMed: 6496779]
- [63]. Saunders A, Strittmatter W, Schmechel D, George-Hyslop PS, Pericak-Vance M, Joo S, Rosi B, Gusella J, Crapper-MacLachlan D, Alberts M, et al. Association of apolipoprotein E allele 4 with late-onset familial and sporadic Alzheimer's disease. *Neurology*. 1993; 43:1467–1467. [PubMed: 8350998]
- [64]. Scheltens P, Leys D, Barkhof F, Huglo D, Weinstein H, Vermersch P, Kuiper M, Steinling M, Wolters EC, Valk J. Atrophy of medial temporal lobes on MRI in "probable" Alzheimer's disease and normal ageing: diagnostic value and neuropsychological correlates. *Journal of Neurology, Neurosurgery & Psychiatry*. 1992; 55:967–972.
- [65]. Shaw LM, Vanderstichele H, Knapiak-Czajka M, Clark CM, Aisen PS, Petersen RC, Blennow K, Soares H, Simon A, Lewczuk P, Dean R, Siemers E, Potter W, Lee VM, Trojanowski JQ, ADNI. Cerebrospinal fluid biomarker signature in Alzheimer's disease neuroimaging initiative subjects. *Annals of Neurology*. 2009; 65:403–413. [PubMed: 19296504]
- [66]. Shi J, Thompson PM, Gutman B, Wang Y. Surface fluid registration of conformal representation: Application to detect disease burden and genetic influence on hippocampus. *NeuroImage*. 2013a; 78:111–134. [PubMed: 23587689]
- [67]. Shi J, Wang Y, Ceschin R, An X, Lao Y, Vanderbilt D, Nelson MD, Thompson PM, Panigrahy A, Leporé N. A multivariate surface-based analysis of the putamen in premature newborns: Regional differences within the ventral striatum. *PloS One*. 2013b; 8:e66736. [PubMed: 23843961]
- [68]. Shi J, Lepor N, Gutman BA, Thompson PM, Baxter LC, Caselli RL, Wang Y, for the Alzheimer's Disease Neuroimaging Initiative. Genetic influence of apolipoprotein E4 genotype on hippocampal morphometry: An N = 725 surface-based Alzheimer's disease neuroimaging initiative study. *Human Brain Mapping*. 2014:3903–3918. [PubMed: 24453132]
- [69]. Sinha D, Chen M-H, Ghosh SK. Bayesian analysis and model selection for interval-censored survival data. *Biometrics*. 1999; 55:585–590. [PubMed: 11318218]
- [70]. Sinha D, Ibrahim JG, Chen MH. A Bayesian Justification of Cox's Partial Likelihood. *Biometrika*. 2003; 90:629–641.
- [71]. Spiegelhalter DJ, Best NG, Carlin BP, Van Der Linde A. Bayesian measures of model complexity and fit. *Journal of the Royal Statistical Society: Series B (Statistical Methodology)*. 2002; 64:583–639.
- [72]. Strittmatter WJ, Saunders AM, Schmechel D, Pericak-Vance M, Enghild J, Salvesen GS, Roses AD. Apolipoprotein E: high-avidity binding to beta-amyloid and increased frequency of type 4

- allele in late-onset familial Alzheimer disease. *Proceedings of the National Academy of Sciences*. 1993; 90:1977–1981.
- [73]. Tabert MH, Manly JJ, Liu X, Pelton GH, Rosenblum S, Jacobs M, Zamora D, Goodkind M, Bell K, Stern Y, Devanand DP. Neuropsychological prediction of conversion to Alzheimer disease in patients with mild cognitive impairment. *Archives of General Psychiatry*. 2006; 63:916–924. [PubMed: 16894068]
- [74]. Tibshirani R. Regression shrinkage and selection via the lasso. *Journal of Royal Statistical Society. Series B*. 1996; 58:267–288.
- [75]. Vemuri P, Gunter JL, Senjem ML, Whitwell JL, Kantarci K, Knopman DS, Boeve BF, Petersen RC, Jack CR Jr. Alzheimer’s disease diagnosis in individual subjects using structural MR images: validation studies. *Neuroimage*. 2008; 39:1186–1197. [PubMed: 18054253]
- [76]. Wang Y, Zhang J, Gutman B, Chan TF, Becker JT, Aizenstein HJ, Lopez OL, Tamburo RJ, Toga AW, Thompson PM. Multivariate tensor-based morphometry on surfaces: application to mapping ventricular abnormalities in HIV/AIDS. *NeuroImage*. 2010; 49:2141–2157. [PubMed: 19900560]
- [77]. Wang Y, Song Y, Rajagopalan P, An T, Liu K, Chou Y-Y, Gutman B, Toga AW, Thompson PM. Surface-based TBM boosts power to detect disease effects on the brain: an N= 804 ADNI study. *Neuroimage*. 2011; 56:1993–2010. [PubMed: 21440071]
- [78]. Yao F, Muller HG, Wang JL. Functional linear regression analysis for longitudinal data. *The Annals of Statistics*. 2005; 33:2873–2903.
- [79]. Young J, Modat M, Cardoso MJ, Mendelson A, Cash D, Ourselin S. Accurate multimodal probabilistic prediction of conversion to Alzheimer’s disease in patients with mild cognitive impairment. *NeuroImage: Clinical*. 2013; 2:735–745. [PubMed: 24179825]
- [80]. Zhang D, Shen D, ADNI. Predicting future clinical changes of MCI patients using longitudinal and multimodal biomarkers. *PLoS One*. 2012; 7:e33182. [PubMed: 22457741]

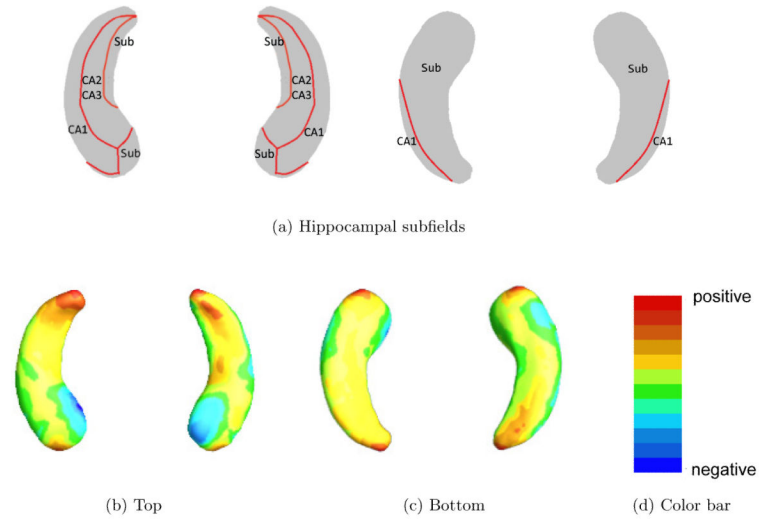


**Fig 1.** ADNI data: panel (a) is hippocampal subfields mapped onto a representative hippocampal surface [4], and panels (b) and (c), respectively, show the top and bottom views of the first subject's hippocampal surface data color-coded by the colorbar in panel (d).

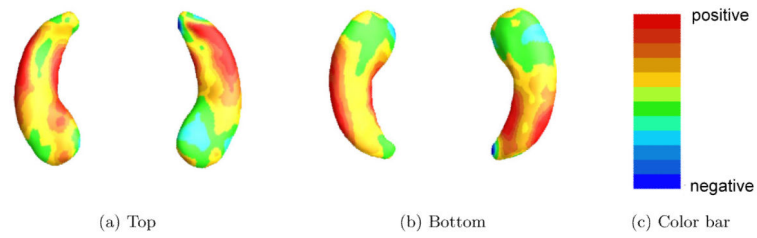


**Fig 2.** ADNI data analysis results for the full BFLCRM model: panels (a) and (b), respectively, show the top and bottom views of the estimated coefficient function associated with the hippocampal surface data color-coded by the colorbar in panel (c).

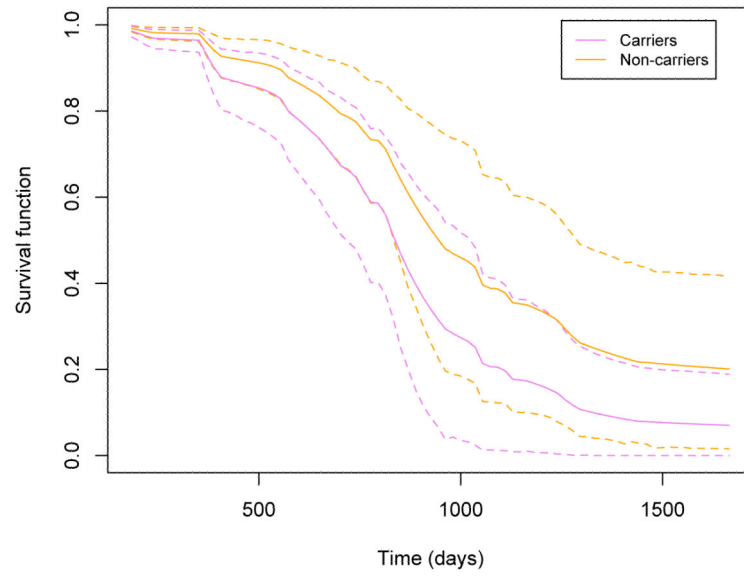


**Fig 3.** ADNI data analysis results: the estimated survival curves of APOE- $\epsilon 4$  carriers and non-carriers under the full BFLCRM model. Other continuous or categorical covariates are fixed at the mean values or reference levels. The dotted lines show the 95% HPD intervals of the estimated survival functions.

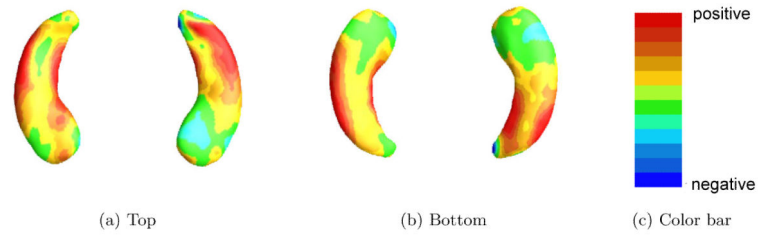


**Fig 4.** ADNI data analysis results for the full BFLCRM model: panels (a) and (b), respectively, show the top and bottom views of the estimated coefficient function associated with the hippocampal surface data color-coded by the colorbar in panel (c).

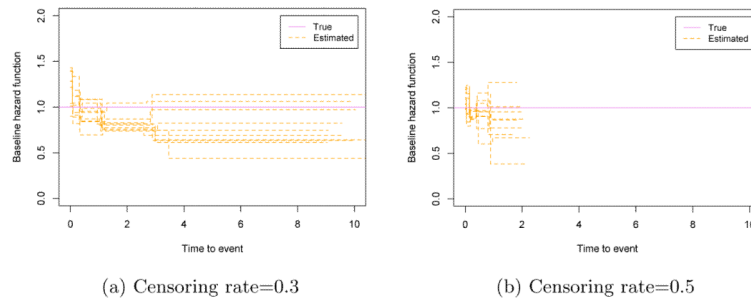


**Fig 5.** Simulation results corresponding to  $h_{01}(\cdot)$ : panels (a) and (b) respectively show the first 10 estimated baseline hazard functions with 0.3 and 0.5 censoring rates based on the size 500 samples. The solid line is the true baseline hazard function,  $h_{01}(\cdot)$ .

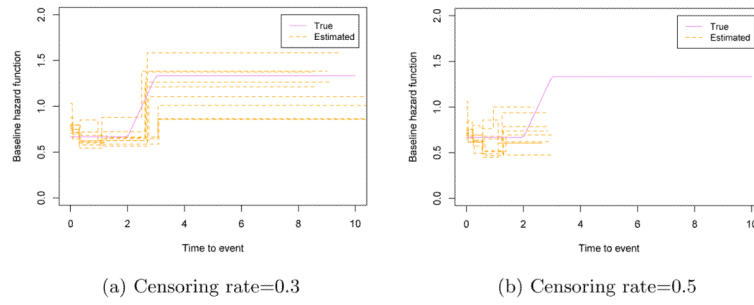


**Fig 6.** Simulation results corresponding to  $h_{02}(\cdot)$ : panels (a) and (b) respectively show the first 10 estimated baseline hazard functions with 0.3 and 0.5 censoring rates based on the size 500 samples. The solid line is the true baseline hazard function,  $h_{02}(\cdot)$ .

**Table 1**

ADNI data analysis results for the full BFLCRM model : the posterior quantities of 19 regression coefficients  $\beta_k$ s, that correspond to  $\mathbf{x}_i$  =(Gender, Handedness, Widowed, Divorced, Never married, Length of Education, Retirement, Age, APOE- $\epsilon$ 4 carrier, ADAS-cog Score, posterior limb of internal capsule, Right hippocampal formation, Left hippocampal formation, Left thalamus, Left amygdala, Right amygdala, and Right thalamus). Mean denotes ‘posterior mean’, SD denotes ‘posterior standard deviation’, and lower and upper, respectively, represent the ‘lower and upper limits’ of a 95% highest posterior density interval.

	$\beta_1$	$\beta_2$	$\beta_3$	$\beta_4$	$\beta_5$	$\beta_6$	$\beta_7$	$\beta_8$
Mean	0.4344	0.2255	0.3119	0.2729	0.7203	-0.0874	0.3455	-0.0519
SD	0.2513	0.3647	0.3827	0.4663	0.7867	0.0367	0.2482	0.0178
lower	-0.0495	-0.5248	-0.4632	-0.6789	-0.9383	-0.1691	-0.0919	-0.0873
upper	0.9478	0.8628	1.0138	1.1195	2.2009	-0.0244	0.8608	-0.0188

	$\beta_9$	$\beta_{10}$	$\beta_{11}$	$\beta_{12}$	$\beta_{13}$	$\beta_{14}$	$\beta_{15}$	$\beta_{16}$	$\beta_{17}$
Mean	0.5550	0.1568	0.0008	0.0006	-0.0011	-0.0004	0.0018	-0.0012	0.0003
SD	0.2341	0.0265	0.0005	0.0004	0.0004	0.0004	0.0009	0.0005	0.0004
lower	0.1258	0.1030	-0.0002	-0.0002	-0.0019	-0.0012	0.0000	-0.0023	-0.0004
upper	1.0258	0.2075	0.0019	0.0014	-0.0004	0.0003	0.0036	-0.0002	0.0010

Author Manuscript

Author Manuscript

Author Manuscript

Author Manuscript

**Table 2**

ADNI data analysis results under the four models: Deviance Information Criterion (DIC) and the empirical means of iAUC values and their corresponding standard errors in the parenthesis calculated from the Monte Carlo cross-validation (MCCV).

	<b>the full BFLCRM model</b>	<b>Model 1</b>	<b>Model 2</b>	<b>Model 3</b>
DIC	427.19	413.08	417.04	438.22
iAUC	0.840 (0.003)	0.836 (0.003)	0.809 (0.003)	0.751 (0.004)

Author Manuscript

Author Manuscript

Author Manuscript

Author Manuscript

ADNI data analysis results for Model 1: the posterior quantities of 12 regression coefficients  $\beta_{kS}$ , that correspond to  $\mathbf{x}_i$ =(Gender, Handedness, Widowed, Divorced, Never married, Length of Education, Retirement, Age, APOE-ε4 carrier, and ADAS-cog Score). Mean denotes 'posterior mean', SD denotes 'posterior standard deviation', and lower and upper, respectively, represent the 'lower and upper limits' of a 95% highest posterior density interval.

**Table 3**

	$\beta_1$	$\beta_2$	$\beta_3$	$\beta_4$	$\beta_5$	$\beta_6$	$\beta_7$	$\beta_8$	$\beta_9$	$\beta_{10}$
Mean	0.3943	0.2826	0.2422	0.1409	0.5174	-0.0577	0.4045	-0.0406	0.5143	0.1572
SD	0.2016	0.3317	0.3121	0.4377	0.7682	0.0341	0.2442	0.0156	0.2190	0.0239
lower	-0.0157	-0.3488	-0.4151	-0.7356	-0.9930	-0.1260	-0.0610	-0.0699	0.1069	0.1104
upper	0.7842	0.9094	0.8308	0.9196	1.9468	0.0045	0.8900	-0.0089	0.9634	0.2030

**Table 4**

Simulation results corresponding to  $h_{01}(\cdot)$  under different censoring rates and sample sizes: the deviance information criterion (DIC), the mean squared errors (MSE) of  $\hat{\beta}$  and  $\hat{\gamma}$  and the estimated integrated area under the curve (iAUCs) and their standard errors in parentheses calculated from the 100 simulated data sets. The Gibbs sampler was run for 20,000 iterations with 5,000 burn-in iterations for each simulated data set.

sample size	censoring rate		MSE $\hat{\beta}$	MSE $\hat{\gamma}$	iAUC	DIC
200	0.3	FPCA	0.109 (0.009)	0.614 (0.016)	0.935 (0.001)	42.99 (3.46)
		PCA	0.113 (0.010)	0.847 (0.020)	0.934 (0.001)	44.66 (3.58)
	0.5	FPCA	0.181 (0.014)	0.696 (0.021)	0.933 (0.002)	-93.80 (3.44)
		PCA	0.186 (0.014)	0.913 (0.025)	0.932 (0.002)	-92.21 (3.46)
500	0.3	FPCA	0.045 (0.003)	0.445 (0.012)	0.932 (0.001)	83.52 (4.52)
		PCA	0.047 (0.003)	0.581 (0.015)	0.930 (0.001)	85.50 (4.57)
	0.5	FPCA	0.052 (0.004)	0.454 (0.013)	0.928 (0.001)	-260.93 (4.58)
		PCA	0.052 (0.004)	0.600 (0.015)	0.927 (0.001)	-259.37 (4.63)

Author Manuscript

Author Manuscript

Author Manuscript

Author Manuscript

**Table 5**

Simulation results corresponding to  $h_{01}(\cdot)$ : the mean iAUC and the corresponding standard error in the parenthesis calculated from the 100 simulated data sets for each scenario. The Gibbs sampler was run for 20,000 iterations with 5,000 burn-in iterations for each simulated data set.

n Censoring rate	200		500	
	0.3	0.5	0.3	0.5
reduced	0.675 (0.004)	0.612 (0.006)	0.668 (0.002)	0.666 (0.002)
full	0.935 (0.001)	0.933 (0.002)	0.932 (0.001)	0.928 (0.001)

Author Manuscript

Author Manuscript

Author Manuscript

Author Manuscript

**Table 6**

Simulation results corresponding to  $h_{02}(\cdot)$  under different censoring rates and sample sizes: the deviance information criterion (DIC), the mean squared errors (MSE) of  $\hat{\beta}$  and  $\hat{\gamma}$  and the estimated integrated area under the curve (iAUC), and their standard errors in parentheses calculated from the 100 simulated data sets. The Gibbs sampler was run for 20,000 iterations with 5,000 burn-in iterations for each simulated data set.

sample size	censoring rate		MSE $\hat{\beta}$	MSE $\hat{\gamma}$	iAUC	DIC
200	0.3	FPCA	0.112 (0.009)	0.618 (0.018)	0.934 (0.001)	128.21 (3.57)
		PCA	0.112 (0.010)	0.854 (0.021)	0.933 (0.001)	129.02 (3.66)
	0.5	FPCA	0.183 (0.017)	0.698 (0.023)	0.933 (0.002)	-15.26 (3.37)
		PCA	0.189 (0.018)	0.913 (0.023)	0.932 (0.002)	-13.70 (3.38)
500	0.3	FPCA	0.048 (0.003)	0.453 (0.012)	0.931 (0.001)	306.94 (4.46)
		PCA	0.049 (0.005)	0.586 (0.015)	0.930 (0.001)	308.62 (4.49)
	0.5	FPCA	0.054 (0.004)	0.457 (0.013)	0.927 (0.001)	-69.55 (4.50)
		PCA	0.054 (0.004)	0.611 (0.016)	0.926 (0.001)	-68.00 (4.54)

Author Manuscript

Author Manuscript

Author Manuscript

Author Manuscript

**Table 7**

Simulation results corresponding to  $h_{02}(\cdot)$ : the mean iAUC and the corresponding standard error in the parenthesis calculated from the 100 simulated data sets for each scenario. The Gibbs sampler was run for 20,000 iterations with 5,000 burn-in iterations for each simulated data set.

n Censoring rate	200		500	
	0.3	0.5	0.3	0.5
reduced	0.673 (0.004)	0.612 (0.006)	0.668 (0.002)	0.665 (0.002)
full	0.934 (0.001)	0.933 (0.002)	0.931 (0.001)	0.927 (0.001)

Author Manuscript

Author Manuscript

Author Manuscript

Author Manuscript